Elucidating the Influence of Anchoring Geometry on the Reactivity of NO_2-Functionalized N-Heterocyclic Carbene Monolayers

Shahar Dery,[†] Suhong Kim,[‡] Gabriele Tomaschun,[§] Iris Berg,[†] Daniel Feferman,[†] Albano Cossaro,[∥] Alberto Verdini,[∥] Luca Floreano,[∥] Thorsten Klüner,[§] F. Dean Toste,*[,‡] and Elad Gross*[,†]

[†]Institute of Chemistry and The Center for Nanoscience and Nanotechnology, The Hebrew University of Jerusalem, Jerusalem 91904, Israel

[‡]Department of Chemistry, University of California, Berkeley, California 94720, United States

[§]Department of Chemistry, Carl von Ossietzky University Oldenburg, 26111 Oldenburg, Germany

[∥]Laboratorio Nazionale TASC, CNR-IOM, Basovizza SS-14, Trieste 34012, Italy

ABSTRACT: The development of chemically addressable N-heterocyclic carbene (NHC) based self-assembled monolayers (SAMs) requires in-depth understanding of the influence of NHC's anchoring geometry on its chemical functionality. Herein, it is demonstrated that the chemical reactivity of surface-anchored NO_2-functionalized NHCs (NO_2–NHCs) can be tuned by modifying the distance between the functional group and the reactive surface, which is governed by the deposition technique. Liquid deposition of NO_2–NHCs on Pt(111) induced a SAM in which the NO_2-aryl groups were flat-lying on the surface. The high proximity between the NO_2 groups and the Pt surface led to high reactivity, and 85% of the NO_2 groups were reduced at room temperature. Lower reactivity was obtained with vapor-deposited NO_2–NHCs that assumed a preferred upright geometry. The separation between the NO_2 groups in the vapor-deposited NO_2–NHCs and the reactive surface circumvented their surface-induced reduction, which was facilitated only after exposure to harsher reducing conditions.

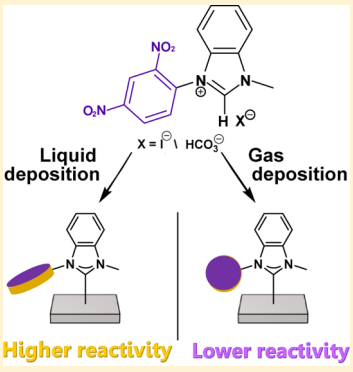

The high chemical tunability and metal affinity of N-heterocyclic carbene molecules (NHCs) have enabled formation of robust NHC-based self-assembled monolayers (SAMs) with exceptional stability and functionality.[1−10] Chemically functionalized NHCs have been utilized for the formation of SAMs with varied application ranges, including molecular patterning, biosensing, and catalysis.[11−16]

Two main approaches have been developed for surface anchoring of NHCs: (1) liquid deposition, in which deprotonation is facilitated by a strong base, such as potassium *tert*-butoxide (KO^{t}Bu), for the formation of an active carbene that can be anchored on metallic surfaces (Scheme 1a)[12,17] and (2) vapor deposition;[1−5,13,15,18] in this approach, hydrogen carbonate counteranions serve as a base for deprotonation of the imidazolium cation, enabling active carbene formation and its surface anchoring under ultrahigh vacuum (UHV) conditions (Scheme 1b).[11]

It was demonstrated that a more homogeneous and better stabilized SAM is formed by vapor deposition, in comparison to the one prepared by liquid deposition.[11,19] However, the influence of the deposition technique on the anchoring geometry of surface-anchored NHCs, which is expected to have a crucial impact on the functionality of chemically addressable NHCs, was not yet elucidated. In this work, we demonstrate that the anchoring geometry has a direct influence on the chemical reactivity of NO_2-functionalized NHCs

Scheme 1. Schematic Illustration of Liquid (a) and Vapor Deposition (b) of NO_2-Functionalized NHCs[1,3,7,8,16,19]

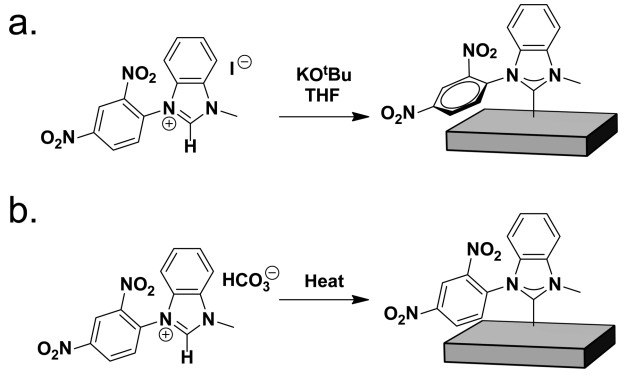

(NO_2–NHCs) and that by changing the deposition technique both the anchoring geometry and chemical reactivity of the NHC-based SAM can be tuned.

Liquid deposition of NO_2–NHCs on Pt(111) was performed by using potassium *tert*-butoxide (KO^{t}Bu) as a base for deprotonation of the tetrahydrofuran (THF) dissolved

imidazolium salt (Scheme 1a). The anchoring geometry, chemical reactivity, and thermal stability of the SAM were identified by conducting X-ray photoelectron spectroscopy (XPS) and near-edge X-ray absorption fine structure (NEXAFS) measurements (performed at the ALOISA beamline of the ELETTRA synchrotron facility in Trieste, Italy),[20,21] along with complementary density functional theory (DFT) calculations. Additional details about the NHC synthesis, the experimental setup and DFT calculations are described in the Supporting Information.

The N 1s XPS signal of liquid-deposited NO_2−NHCs on Pt(111) is shown in Figure 1a. The wide (fwhm = 3 eV) low-

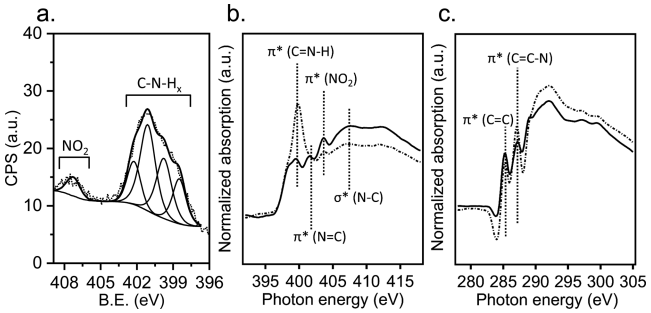

Figure 1. Spectroscopic characterization of liquid-deposited NO_2−NHC on Pt(111). (a) N 1s XPS spectrum. (b) Nitrogen k-edge NEXAFS spectra. (c) Carbon k-edge NEXAFS spectra. NEXAFS spectra were acquired at both p- and s-polarization (marked by solid and dotted lines, respectively).

energy peak (397−404 eV) revealed the presence of various nitrogen species on the surface. The peak was fit by four Gaussians centered at 398.5, 399.8, 401.1, and 402.3 eV, which were assigned to pyridinic (C−N═C), amine (C−NH_2/C═NH), pyrrolic (N═C), and protonated amine (−NH_3^+), respectively.[22−25]

The high-energy N 1s XPS peak (406−409 eV) was fit by one Gaussian and correlated to NO_2 species. The low- to high-energy N 1s XPS peak area ratio was 1:10, while the expected ratio based on the molecular structure of NO_2−NHC was 1:1. This ratio indicates that 85% of the NO_2 groups in the liquid-deposited NO_2-NHCs were reduced (Table 1). The XPS

Table 1. XPS Peak Area Analysis

		N_{1s}/Pt_{4f}	C_{1s}/Pt_{4f}	C_{1s}/N_{1s}	NO_2:NH_x
liquid deposition	as-deposited	0.06	0.35	5.48	15:85
vapor deposition	as-deposited	0.04	0.11	3.05	40:60
	after reduction	0.04	0.10	2.97	5:95

results revealed that partial decomposition and nitro-group reduction occurred following liquid deposition of NO_2−NHCs on the Pt surface. These two processes were facilitated by residue H_2 molecules, which were the main gas component in the UHV chamber.

Nitrogen and carbon k-edge NEXAFS measurements (Figure 1b,c, respectively) were conducted at both p- and s-polarization (marked by solid and dotted lines, respectively) to determine the anchoring geometry of liquid-deposited NO_2−NHCs. The p-polarized nitrogen k-edge NEXAFS spectrum (solid line, Figure 1b) displayed three dominant peaks in the π^* region (395−405 eV). The peak at 403.6 eV was correlated to N 1s → $\pi^*_{(NO2)}$ transitions, while the peak at 401.5 eV was assigned to the N 1s → $\pi^*_{(N=C)}$ transition and the peak at 399.7 eV was correlated to the N 1s → $\pi^*_{(C=N-H)}$ transition.[26,27] Interestingly, the s-polarized spectrum (dotted line) revealed a much more intense N 1s → $\pi^*_{(C=N-H)}$ transition, while the N 1s → $\pi^*_{(NO2)}$ transition peak was higher in the p-polarized spectrum. These differences indicate that the −NO_2 groups obtained a preferred parallel orientation to the surface, while the reduced groups were mostly oriented perpendicularly to the surface. The p- and s-polarized carbon k-edge NEXAFS spectra of liquid-deposited NO_2−NHCs (solid and dotted lines in Figure 1c, respectively) included two π^* transitions at 285.3 and 286.5 eV corresponding to C 1s → $\pi^*_{(C=C)}$ and $\pi^*_{(C=C-N)}$ transitions, respectively.[27,28] The two π^* transition peaks were almost identical in their position and amplitudes in both the p- and s-polarized spectra.

DFT calculations were conducted to identify the preferred anchoring geometry and adsorption energy of liquid-deposited NHCs on a Pt(111) surface and a Pt(111) surface decorated with a Pt adatom (Pt-ad/Pt(111)) (Figure 2a and Supporting

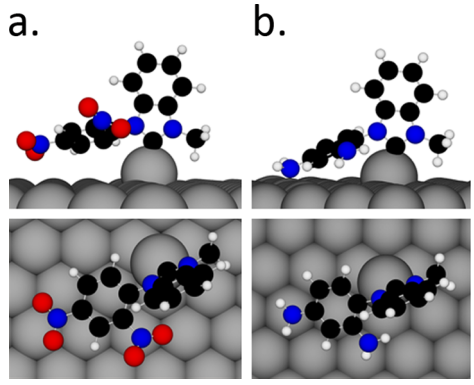

Figure 2. DFT calculations of the optimized adsorption geometry of NO_2−NHC (a) and NH_2−NHC (b) on Pt-ad/Pt(111) (the Pt(111) surface decorated with a Pt adatom). Side and top views of the NHCs are shown (top and bottom panels, respectively).

Information Figure S1). The optimal anchoring site for NO_2−NHCs was on the adatom (E_{ads} = −4.94 eV), in which the NO_2-aryl orientation was mostly flat-lying on the surface, while the imidazole ring was oriented in a standing position (see further adsorption analysis in Supporting Information Figure S1). The DFT results nicely corroborate the experimental data, revealing that the similarities between the p- and s-polarized carbon NEXAFS spectra are due to the fact that the two phenyl rings are positioned at 90° to each other. It should be noted that DFT calculations identified that reduction of the −NO_2 groups does not noticeably influence the NHC anchoring geometry (Figures 2b and S1). The identification of the Pt adatom as the most favorable adsorption site for NO_2−NHCs on the Pt(111) surface indicates that NO_2−NHC adsorption will lead to restructuring of the Pt surface.[3,7,29]

Vapor deposition of NO_2−NHCs on the Pt(111) surface was conducted under UHV conditions by thermal evaporation of NO_2-fucntionalized carbonate-imidazolium salt (Scheme 1b).[30] The N 1s XPS spectrum of vapor-deposited NO_2−NHCs on Pt(111) is shown in Figure 3a (black colored spectrum). The low-energy N 1s XPS peak was constructed of

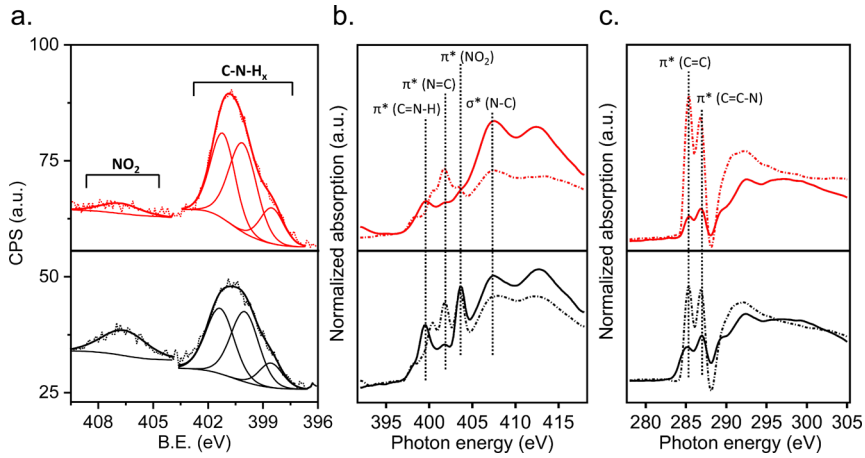

Figure 3. Spectroscopic characterization of vapor-deposited NO_2−NHCs on Pt(111) before (black colored spectrum) and after (red colored spectrum) exposure to 1000 L of H_2 at 100 °C. (a) N 1s XPS spectrum. (b) Nitrogen k-edge NEXAFS spectra. (c) Carbon k-edge NEXAFS spectra. NEXAFS spectra were acquired at both p- and s-polarization (marked by solid and dotted lines, respectively).

two dominant Gaussians, as expected from the molecular structure of the NO_2−NHC. The low- to high-energy N 1s XPS peak area ratio in vapor-deposited NO_2−NHCs was 1:5, indicating that 60% of the NO_2 groups were reduced upon NHC deposition (Table 1). These results reveal that NO_2−NHCs that were anchored on the surface by vapor deposition show lower affinity toward $-NO_2$ reduction and partial decomposition, in comparison to NO_2−NHCs that were liquid-deposited on the Pt surface. On the basis of these results, it can be deduced that vapor deposition is a less destructive technique, in comparison to liquid deposition, for surface anchoring of NO_2−NHCs.

The anchoring-geometry of vapor-deposited NHCs was analyzed by conducting nitrogen and carbon k-edge NEXAFS measurements (Figure 3b,c, respectively). The p-polarized nitrogen k-edge NEXAFS spectrum (solid line, black colored spectrum in Figure 3b) showed two intense peaks in the π^* transition range, correlated to N 1s → $\pi^*_{(NO2)}$ (403.6 eV) and N 1s → $\pi^*_{(C=N-H)}$ (399.7 eV) transitions. However, the position and amplitude of the N 1s → $\pi^*_{(NO2)}$ transition was almost identical in both p- and s-polarized spectra (solid and dotted black colored spectra, respectively, Figure 3b). The s-polarized spectrum showed an additional peak at 401.5 eV, correlated to the N 1s → $\pi^*_{(N=C)}$ transition. This peak was not detected in the p-polarized spectrum. The σ^* transition range (405−415 eV) was similar in its pattern and amplitude in both p- and s-polarized spectra.

Clear differences were obtained between the p- and s-polarized carbon k-edge NEXAFS spectra of vapor-deposited NHCs (solid and dotted black colored spectra, respectively, Figure 3c). The dichroism implies that the C=C and C=C−N bonds constructing the benzimidazolium and NO_2-aryl rings have a preferred standing orientation. Thus, integration of the carbon and nitrogen NEXAFS results indicates that, unlike liquid-deposited NHCs, the vapor-deposited NHCs showed a preferred perpendicular orientation to the surface.

DFT calculations revealed that the perpendicular orientation was preferred once the surface density of NO_2−NHCs was increased (Figures 4a and S2). The stabilizing intermolecular π−π interactions between neighboring standing NO_2−NHCs compensated the weaker interaction between the Pt surface and the surface-anchored molecules in a standing position (E_{ads} = −4.35 eV). Due to steric hindrance, similar intermolecular

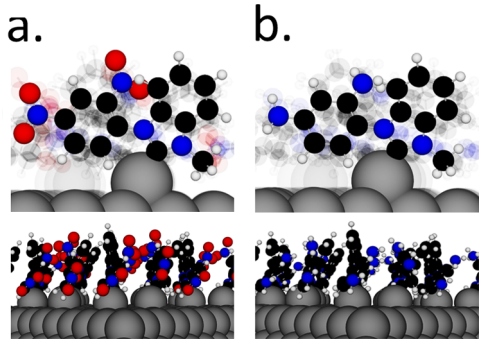

Figure 4. DFT calculations of the optimized adsorption geometry of NO_2−NHC (a) and NH_2−NHCs (b) on Pt-ad/Pt(111), which included intermolecular interactions. The lighter shading of other adsorbates on the surface illustrates the higher surface coverage, which is described in more detail in Figure S2. Front and side views of the surface-anchored NHCs are shown (top and bottom panels, respectively).

π−π interactions cannot be formed between the imidazole rings of NHCs that were anchored on the surface with their nitroaryl group in a flat-lying position.

Integration of the experimental results and theoretical calculations specify that vapor deposition enabled the formation of a highly packed monolayer with strong intermolecular interactions in which the two NHC rings were oriented in a close to standing position. The high packing density of a monolayer constructed of NO_2−NHCs in a standing position makes it energetically favorable over a monolayer of flat-lying NO_2−NHCs, characterized with lower packing density due to steric hindrance.

The reasons for the formation of a monolayer of flat-lying NO_2−NHCs with lower packing density by the liquid deposition approach can be correlated to either the presence of base residues on the surface or the presence of encapsulated solvent molecules. The presence of potassium residues on the Pt surface, following liquid deposition of NO_2-NHCs, was identified in the carbon k-edge NEXAFS measurements (Figure 1c) in which two peaks at 296 and 298 eV were detected and correlated with potassium. The source for potassium was the KO^{t}Bu that was used as a base in the liquid deposition (Scheme 1a). The distribution of potassium

and assumingly also $^{t}BuO^{-}$ on the Pt surface will limit the surface diffusivity of NHCs and thus hamper the formation of an ordered SAM with high packing density.[31,32]

Strong interactions between the activated NHCs and the THF molecules are required for dissolving the NHCs in the solution phase. These interactions can lead to the presence of entrapped solvent molecules on the surface that will limit the surface diffusivity and modify the anchoring geometry of surface-anchored NHCs. It was previously demonstrated that the packing density and anchoring geometry of thiol-based SAMs were influenced by the properties of the solvent that was used in the deposition process.[33,34] Indication for the presence of entrapped solvent molecules in the liquid-deposited monolayer was identified in quantitative analysis of the XPS spectra (Table 1). The C 1s/N 1s ratio in vapor-deposited NHCs was 3.05, which is comparable to the expected 3.5 carbon to nitrogen ratio in NO_2−NHC. However, the C 1s/N 1s ratio in the liquid-deposited NO_2−NHCs was 5.48, which is higher by 60% than the expected ratio. These results can be connected with the presence of encapsulated solvent molecules in the liquid-deposited NHC-based SAM. The encapsulation of solvent molecules in the SAM would hinder the formation of a monolayer with high packing density. The low packing density of NO_2−NHCs on the Pt surface will eventually induce a preferred flat-lying position of the nitroaryl substituents.

The variations in the anchoring geometry of vapor- and liquid-deposited NO_2−NHCs changed the distance between the $-NO_2$ groups and the reactive Pt surface. These differences impact the affinity toward surface-induced reduction of the $-NO_2$ groups (Table 1). Higher probability toward nitro reduction was coupled with shorter distances and stronger interaction between the nitro groups and Pt surface. Thus, nitro reduction was facilitated in liquid-deposited NHCs, in which the two $-NO_2$ groups reside in high proximity to the Pt surface (Figure 2a). Lower tendency toward $-NO_2$ reduction was obtained in vapor-deposited NHCs, characterized with larger distances between the ortho $-NO_2$ group and the Pt surface (Figure 4a).

To identify the influence of reducing conditions on the anchoring geometry and nitro-group reducibility, the vapor-deposited NO_2−NHCs were exposed to 1000 L (L = Langmuir ; 1 L = 10^{-6} Torr·s) of H_2 at 100 °C. N 1s XPS measurement revealed that the high-energy peak was quenched following exposure of the vapor-deposited NHCs to reducing conditions (red colored spectrum, Figure 3a). XPS peak area ratio analysis showed that the $-NO_2$ reduction yield was increased from 60 to 95% following exposure to harsher reducing conditions (Table 1). The surface density of the NHCs did not noticeably change after exposure to reducing conditions, as obtained by the constant N 1s/Pt 4f ratio (Table 1), thus excluding any reduction-induced desorption of surface-anchored NHCs.

Nitrogen k-edge NEXAFS spectra (red colored spectra, Figure 3b) showed that the N 1s → $\pi^*_{(NO2)}$ (403.6 eV) and N 1s → $\pi^*_{(C=N-H)}$ (399.7 eV) transitions were quenched after exposure to reducing conditions. These changes indicate that most of the nitro groups were fully reduced to amine following exposure to reducing conditions. Interestingly, a noticeable increase in the carbon k-edge dichroism was observed after exposure of the vapor-deposited NO_2−NHCs to reducing conditions (red colored spectra, Figure 3c). The changes in the NEXAFS spectra revealed that the anchoring geometry of the NHCs was shifted to a more perpendicular position following NO_2 reduction. DFT calculations identified that nitro -group reduction led to reorientation of the NHCs' aromatic rings into a more upright position (Figures 4b and S2). This is due to the fact that NO_2 reduction lowered the steric hindrance between the surface-anchored molecules, thus further enabling them to assume an optimized orientation.

In conclusion, the influence of anchoring geometry on the chemical reactivity of surface-anchored NO_2−NHCs was demonstrated by modifying the NHC deposition technique. Liquid deposition of NO_2−NHCs induced the formation of a SAM in which the nitroaryl groups were flat-lying on the Pt surface. At this anchoring geometry, the NO_2 reduction was facilitated under mild conditions due to the high proximity between the NO_2 groups and the Pt surface. Vapor deposition led to the formation of NHC-based SAMs in which the NHCs assumed a favored standing orientation. The separation between the reactive surface and the NO_2 groups in the vapor-deposited NHCs circumvented their surface-induced reduction under mild conditions. The results presented herein demonstrate the impact of the distance between functional groups and the reactive surface on the reactivity of chemically addressable SAMs. The anchoring geometry is therefore identified as a crucial factor that should be taken into consideration in the design of chemically addressable SAMs.

■ ASSOCIATED CONTENT

Supporting Information

The Supporting Information is available free of charge on the ACS Publications website at DOI: 10.1021/acs.jpclett.9b01808.

Additional DFT calculations and details about the experimental setup (PDF)

■ AUTHOR INFORMATION

Corresponding Authors

*E-mail: fdtoste@berkeley.edu (F.D.T.).
*E-mail: elad.gross@mail.huji.ac.il (E.G.).

ORCID

Albano Cossaro: 0000-0002-8429-1727
Alberto Verdini: 0000-0001-8880-2080
Luca Floreano: 0000-0002-3654-3408
Thorsten Klüner: 0000-0003-1389-6013
F. Dean Toste: 0000-0001-8018-2198
Elad Gross: 0000-0002-8330-7299

Notes

The authors declare no competing financial interest.

■ ACKNOWLEDGMENTS

This research was partially supported by the European Research Council (ERC) under the European Union's Horizon 2020 research and innovation program (Grant Agreement No. 802769, ERC Starting Grant "MapCat") and by the State of Lower Saxony, Hannover, Germany. S.D. acknowledges financial support from the Israeli Ministry of Energy and the Azrieli foundation. F.D.T. thanks the Director, Office of Science, Office of Basic Energy Sciences and the Division of Chemical Sciences, Geosciences, and Biosciences of the U.S. Department of Energy at LBNL (DE-AC02-05CH11231) for partial support of this work. The theoretical calculations were performed at the HPC Clusters HERO and CARL, located at the University of Oldenburg and funded by

the DFG through its Major Research Instrumentation Program (INST 184/108-1 FUGG and INST 184/157-1 FUGG) and the Ministry of Science and Culture of the Lower Saxony State. Computational analysis was also performed at the North-German Supercomputing Alliance (HLRN), within the project: nic00030.

REFERENCES

(1) Zhukhovitskiy, A. V.; Mavros, M. G.; Van Voorhis, T.; Johnson, J. A. Addressable carbene anchors for gold surfaces. *J. Am. Chem. Soc.* **2013**, *135*, 7418−7421.

(2) Crudden, C. M.; Horton, J. H.; Ebralidze, I. I.; Zenkina, O. V.; McLean, A. B.; Drevniok, B.; She, Z.; Kraatz, H.-B.; Mosey, N. J.; Seki, T.; et al. Ultra stable self-assembled monolayers of N-heterocyclic carbenes on gold. *Nat. Chem.* **2014**, *6*, 409−414.

(3) Bakker, A.; Timmer, A.; Kolodzeiski, E.; Freitag, M.; Gao, H. Y.; Mönig, H.; Amirjalayer, S.; Glorius, F.; Fuchs, H. Elucidating the Binding Modes of N-Heterocyclic Carbenes on a Gold Surface. *J. Am. Chem. Soc.* **2018**, *140*, 11889−11892.

(4) Li, Z.; Narouz, M. R.; Munro, K.; Hao, B.; Crudden, C. M.; Horton, J. H.; Hao, H. Carboxymethylated Dextran-Modified N-Heterocyclic Carbene Self-Assembled Monolayers on Gold for Use in Surface Plasmon Resonance Biosensing. *ACS Appl. Mater. Interfaces* **2017**, *9*, 39223−39234.

(5) Lv, A.; Freitag, M.; Chepiga, K. M.; Schäfer, A. H.; Glorius, F.; Chi, L. N-Heterocyclic-Carbene-Treated Gold Surfaces in Pentacene Organic Field-Effect Transistors: Improved Stability and Contact at the Interface. *Angew. Chem., Int. Ed.* **2018**, *57*, 4792−4796.

(6) Weidner, T.; Baio, J. E.; Mundstock, A.; Große, C.; Karthäuser, S.; Bruhn, C.; Siemeling, U. NHC-based self-assembled monolayers on solid gold substrates. *Aust. J. Chem.* **2011**, *64*, 1177−1179.

(7) Lovat, G.; Doud, E. A.; Lu, D.; Kladnik, G.; Inkpen, M. S.; Steigerwald, M. L.; Cvetko, D.; Hybertsen, M. S.; Morgante, A.; Roy, X.; et al. Determination of the structure and geometry of N-heterocyclic carbenes on Au (111) using high-resolution spectroscopy. *Chem. Sci.* **2019**, *10*, 930−935.

(8) Larrea, C. R.; Baddeley, C. J.; Narouz, M. R.; Mosey, N. J.; Horton, J. H.; Crudden, C. M. N-Heterocyclic Carbene Self-assembled Monolayers on Copper and Gold: Dramatic Effect of Wingtip Groups on Binding Orientation and Assembly. *ChemPhysChem* **2017**, *18*, 3536−3539.

(9) Crespo, J.; Guari, Y.; Ibarra, A.; Larionova, J.; Lasanta, T.; Laurencin, D.; López-de-Luzuriaga, J. M.; Monge, M.; Olmos, M. E.; Richeter, S. Ultrasmall NHC-coated gold nanoparticles obtained through solvent free thermolysis of organometallic Au(i) complexes. *Dalton Trans.* **2014**, *43*, 15713−15718.

(10) Rodríguez-Castillo, M.; Lugo-Preciado, G.; Laurencin, D.; Tielens, F.; van der Lee, A.; Clément, S.; Guari, Y.; López-de-Luzuriaga, J. M.; Monge, M.; Remacle, F.; et al. Experimental and Theoretical Study of the Reactivity of Gold Nanoparticles Towards Benzimidazole-2-ylidene Ligands. *Chem. - Eur. J.* **2016**, *22*, 10446−10458.

(11) Crudden, C. M.; Horton, J. H.; Narouz, M. R.; Li, Z.; Smith, C. A.; Munro, K.; Baddeley, C. J.; Larrea, C. R.; Drevniok, B.; Thanabalasingam, B.; et al. Simple direct formation of self-assembled N-heterocyclic carbene monolayers on gold and their application in biosensing. *Nat. Commun.* **2016**, *7*, 12654.

(12) Wu, C.-Y.; Wolf, W. J.; Levartovsky, Y.; Bechtel, H. A.; Martin, M. C.; Toste, F. D.; Gross, E. High-spatial-resolution mapping of catalytic reactions on single particles. *Nature* **2017**, *541*, 511−515.

(13) Levratovsky, Y.; Gross, E. High spatial resolution mapping of chemically-active self-assembled N-heterocyclic carbenes on Pt nanoparticles. *Faraday Discuss.* **2016**, *188*, 345−353.

(14) Dery, S.; Amit, E.; Gross, E. Identifying catalytic reactions on single nanoparticles. *Top. Catal.* **2018**, *61*, 923−939.

(15) Nguyen, D. T.; Freitag, M.; Körsgen, M.; Lamping, S.; Rühling, A.; Schaefer, A. H.; Siekman, M. H.; Arlinghaus, H. F.; van der Wiel, W. G.; Glorius, F.; et al. Versatile Micropatterns of N-Heterocyclic Carbenes on Gold Surfaces: Increased Thermal and Pattern Stability with Enhanced Conductivity. *Angew. Chem., Int. Ed.* **2018**, *57*, 11465−11469.

(16) DeJesus, J. F.; Trujillo, M. J.; Camden, J. P.; Jenkins, D. M. N-Heterocyclic Carbenes as a Robust Platform for Surface-Enhanced Raman Spectroscopy. *J. Am. Chem. Soc.* **2018**, *140*, 1247−1250.

(17) Dery, S.; Kim, S.; Haddad, D.; Cossaro, A.; Verdini, A.; Floreano, L.; Toste, F. D.; Gross, E. Identifying site-dependent reactivity in oxidation reactions on single Pt particles. *Chem. Sci.* **2018**, *9*, 6523−6531.

(18) Dery, S.; Kim, S.; Tomaschun, G.; Haddad, D.; Cossaro, A.; Verdini, A.; Floreano, L.; Klüner, T.; Toste, F.; Gross, E. Flexible NO2-Functionalized N-Heterocyclic Carbene Monolayers on Au (111) Surface *Chem. Eur. J.* [Online early access]. DOI: 10.1002/chem.201903434. Published online: Aug 8, **2019**. https://onlinelibrary.wiley.com/doi/abs/10.1002/chem.201903434.

(19) Wang, G.; Rühling, A.; Amirjalayer, S.; Knor, M.; Ernst, J. B.; Richter, C.; Gao, H.-J.; Timmer, A.; Gao, H.-Y.; Doltsinis, N. L.; Glorius, F.; Fuchs, H. Ballbot-type motion of N-heterocyclic carbenes on gold surfaces. *Nat. Chem.* **2017**, *9*, 152.

(20) Busetto, E.; Lausi, A.; Bernstorff, S. The high-energy monochromator for the ALOISA beamline at Elettra. *Rev. Sci. Instrum.* **1995**, *66*, 2078−2081.

(21) Floreano, L.; Naletto, G.; Cvetko, D.; Gotter, R.; Malvezzi, M.; Marassi, L.; Morgante, A.; Santaniello, A.; Verdini, A.; Tommasini, F.; Tondello, G. Performance of the grating-crystal monochromator of the ALOISA beamline at the Elettra Synchrotron. *Rev. Sci. Instrum.* **1999**, *70*, 3855−3864.

(22) Cossaro, A.; Dell'Angela, M.; Verdini, A.; Puppin, M.; Kladnik, G.; Coreno, M.; de Simone, M.; Kivimäki, A.; Cvetko, D.; Canepa, M.; Floreano, L. Amine Functionalization of Gold Surfaces: Ultra High Vacuum Deposition of Cysteamine on Au(111). *J. Phys. Chem. C* **2010**, *114*, 15011−15014.

(23) Song, X.; Ma, Y.; Wang, C.; Dietrich, P. M.; Unger, W. E. S.; Luo, Y. Effects of Protonation, Hydrogen Bonding, and Photodamaging on X-ray Spectroscopy of the Amine Terminal Group in Aminothiolate Monolayers. *J. Phys. Chem. C* **2012**, *116*, 12649−12654.

(24) Wang, J.; Neoh, K. G.; Kang, E. T. Comparative study of chemically synthesized and plasma polymerized pyrrole and thiophene thin films. *Thin Solid Films* **2004**, *446*, 205−217.

(25) Jansen, R. J. J.; van Bekkum, H. XPS of nitrogen-containing functional groups on activated carbon. *Carbon* **1995**, *33*, 1021−1027.

(26) Graf, N.; Yegen, E.; Gross, T.; Lippitz, A.; Weigel, W.; Krakert, S.; Terfort, A.; Unger, W. E. S. XPS and NEXAFS studies of aliphatic and aromatic amine species on functionalized surfaces. *Surf. Sci.* **2009**, *603*, 2849−2860.

(27) La, Y.-H.; Jung, Y. J.; Kang, T.-H.; Ihm, K.; Kim, K.-J.; Kim, B.; Park, J. W. NEXAFS Studies on the Soft X-ray Induced Chemical Transformation of a 4-Nitrobenzaldimine Monolayer. *Langmuir* **2003**, *19*, 9984−9987.

(28) Siemeling, U.; Memczak, H.; Bruhn, C.; Vogel, F.; Träger, F.; Baio, J.; Weidner, T. Zwitterionic dithiocarboxylates derived from N-heterocyclic carbenes: coordination to gold surfaces. *Dalton Trans.* **2012**, *41*, 2986−2994.

(29) Jiang, L.; Zhang, B.; Médard, G.; Seitsonen, A. P.; Haag, F.; Allegretti, F.; Reichert, J.; Kuster, B.; Barth, J. V.; Papageorgiou, A. C. N-Heterocyclic carbenes on close-packed coinage metal surfaces: bis-carbene metal adatom bonding scheme of monolayer films on Au, Ag and Cu. *Chem. Sci.* **2017**, *8*, 8301−8308.

(30) Zeng, Y.; Zhang, T.; Narouz, M. R.; Crudden, C. M.; McBreen, P. H. Generation and conversion of an N-heterocyclic carbene on Pt(111). *Chem. Commun.* **2018**, *54*, 12527−12530.

(31) Tamada, K.; Hara, M.; Sasabe, H.; Knoll, W. Surface Phase Behavior of n-Alkanethiol Self-Assembled Monolayers Adsorbed on Au(111): An Atomic Force Microscope Study. *Langmuir* **1997**, *13*, 1558−1566.

(32) Dannenberger, O.; Buck, M.; Grunze, M. Self-Assembly of n-Alkanethiols: A Kinetic Study by Second Harmonic Generation. *J. Phys. Chem. B* **1999**, *103*, 2202−2213.
(33) Anderson, M. R.; Evaniak, M. N.; Zhang, M. Influence of Solvent on the Interfacial Structure of Self-Assembled Alkanethiol Monolayers. *Langmuir* **1996**, *12*, 2327−2331.
(34) Dai, J.; Li, Z.; Jin, J.; Cheng, J.; Kong, J.; Bi, S. Study of the solvent effect on the quality of dodecanethiol self-assembled monolayers on polycrystalline gold. *J. Electroanal. Chem.* **2008**, *624*, 315−322.